Molecular Neurobiology (2023) 60:2379–2396
https://doi.org/10.1007/s12035-022-03129-2

BMSC-Derived Exosomes Carrying lncRNA-ZFAS1 Alleviate Pulmonary Ischemia/Reperfusion Injury by UPF1-Mediated mRNA Decay of FOXD1

Cao Gao[1] · Yan-Jie Xu[2] · Zhi-xiu Meng[1] · Shuang Gu[3] · Lei Zhang[3] · Liang Zheng[3]

Received: 25 April 2022 / Accepted: 4 November 2022 / Published online: 18 January 2023

Abstract

Bone marrow-derived mesenchymal stem cells (BMSCs) exert protective effects against pulmonary ischemia/reperfusion (I/R) injury; however, the potential mechanism involved in their protective ability remains unclear. Thus, this study aimed to explore the function and underlying mechanism of BMSC-derived exosomal lncRNA-ZFAS1 in pulmonary I/R injury. Pulmonary I/R injury models were established in mice and hypoxia/reoxygenation (H/R)-exposed primary mouse lung microvascular endothelial cells (LMECs). Exosomes were extracted from BMSCs. Target molecule expression was assessed by qRT-PCR and Western blotting. Pathological changes in the lungs, pulmonary edema, apoptosis, pro-inflammatory cytokine levels, SOD, MPO activities, and MDA level were measured. The proliferation, apoptosis, and migration of LMECs were detected by CCK-8, EdU staining, flow cytometry, and scratch assay. Dual-luciferase reporter assay, RNA pull-down, RIP, and ChIP assays were performed to validate the molecular interaction. In the mouse model of pulmonary I/R injury, BMSC-Exos treatment relieved lung pathological injury, reduced lung W/D weight ratio, and restrained apoptosis and inflammation, whereas exosomal ZFAS1 silencing abolished these beneficial effects. In addition, the proliferation, migration inhibition, apoptosis, and inflammation in H/R-exposed LMECs were repressed by BMSC-derived exosomal ZFAS1. Mechanistically, ZFAS1 contributed to FOXD1 mRNA decay via interaction with UPF1, thereby leading to Gal-3 inactivation. Furthermore, FOXD1 depletion strengthened the weakened protective effect of ZFAS1-silenced BMSC-Exos on pulmonary I/R injury. ZFAS1 delivered by BMSC-Exos results in FOXD1 mRNA decay and subsequent Gal-3 inactivation via direct interaction with UPF1, thereby attenuating pulmonary I/R injury.

Keywords Pulmonary I/R injury · Mesenchymal stem cells · Exosomes · lncRNA-ZFAS1 · FOXD1 signaling

Abbreviations

ANOVA	Analysis of variance
BMSC-Exos	BMSC-derived exosomes
BMSCs	Bone marrow-derived MSCs
CCK-8	Cell counting kit 8
ChIP	Chromatin immunoprecipitation
DAPI	4′-6-Diamidino-2-phenylindole
EdU	5-Ethynyl-2′-deoxyuridine
FBS	Fetal bovine serum
FOXD1	Forkhead box D1
Gal-3	Galectin-3
H&E	Hematoxylin and eosin
HLA-DR	Human leukocyte antigen DR
H/R	Hypoxia/reoxygenation
Hsp70	Heat shock protein
I/R	Ischemia/reperfusion
LMECs	Lung microvascular endothelial cells
lncRNAs	Long non-coding RNAs
MEG3	Maternally expressed gene 3
MSCs	Mesenchymal stem cells
NTA	Nanoparticle tracking analysis
PBS	Phosphate-buffered saline
PTBP1	Polypyrimidine tract-binding protein 1

✉ Liang Zheng
zhengliang1019@163.com

[1] Departments of Anesthesiology, The Third Affiliated Hospital of Soochow University, Changzhou 213000, Jiangsu Province, People's Republic of China

[2] Departments of Oncology, The Third Affiliated Hospital of Soochow University, Changzhou 213000, Jiangsu Province, People's Republic of China

[3] Department of Thoracic Surgery, The Third Affiliated Hospital of Soochow University, No. 185, Juqian Road, Changzhou 213000, Jiangsu Province, People's Republic of China

qRT-PCR	Quantitative real-time PCR
RBPs	RNA-binding proteins
RIP	RNA immunoprecipitation
shNC	Negative control shRNA
TSG101	Tumor susceptibility gene 101
TUNEL	Terminal deoxynucleotidyl transferase-mediated dUTP nick end-labeling
UPF1	Up-frameshift 1
W/D	Wet/dry
XIST	X-inactive-specific transcript
ZFAS1	Zinc finger antisense 1
ZFPM2-AS1	Zinc finger protein multitype 2 antisense RNA 1

Introduction

Lung ischemia and succeeding reperfusion refer to pulmonary ischemia/reperfusion (I/R) injury, which occurs during many clinical events, including heart or lung transplantation, cardiopulmonary bypass surgery, and pulmonary thrombolysis [1]. Pulmonary I/R injury remains a serious problem that induces primary graft dysfunction, which has been considered as a primary cause of death after lung transplantation [1, 2]. In addition, pulmonary I/R injury results in the overproduction of reactive oxygen species, thereby causing direct endothelial cell injury, apoptosis, and inflammatory response [3]. Recent studies have reported multiple treatment strategies to limit pulmonary I/R injury, such as anti-oxidant strategies, anti-inflammatory strategies, gaseous molecular ventilation, and application of mesenchymal stem cells (MSCs) [4]. Despite extensive study, the exact pathological mechanism of pulmonary I/R injury remains unclear, and a satisfactory treatment is not yet available. Therefore, uncovering the potential molecular mechanism of pulmonary I/R injury is essential to develop novel effective clinical interventions.

Growing evidence has demonstrated the protective effect of MSCs against lung injury after lung transplantation [5, 6]. MSCs induce protection against lung injury by releasing many paracrine factors that inhibit apoptosis, inflammation, and epithelial and endothelial leakage [5]. In addition, exosomes released by MSCs play a crucial role in the therapeutic efficacy of MSCs during myocardial repair [7]. Exosomes are small membrane vesicles of 30–150 nm length, which mediate the intercellular communication by delivering functional proteins and RNAs [8]. Previous reports have suggested that bone marrow-derived MSC exosomes (BMSC-Exos) relieved pulmonary I/R injury [9, 10], which possessed similar physiological functions to BMSCs. Notably, exosomes have distinct advantages over MSCs because of the absence of immune rejection [8], indicating that BMSC-Exos have a broader application potential than BMSCs after lung transplantation. However, the protective mechanism of BMSC-Exos underlying pulmonary I/R injury remains unknown.

Long non-coding RNAs (lncRNAs) are RNA transcripts composed of more than 200 nucleotides without coding capacity, which participate in multiple pathophysiologic processes such as cell differentiation, growth, inflammation, neuronal differentiation, or cancer development through different mechanisms of gene regulation [11–13]. For example, lncRNA X-inactive-specific transcript was reported to be involved in acute lung injury after lung transplantation via sponging miR-21 [14]. A recent study has indicated that lncRNA zinc finger antisense 1 (ZFAS1) could attenuate septic lung injury via repressing inflammation [15], indicating the application potential of ZFAS1 in relieving pulmonary I/R injury. Recently, the exosome-mediated delivery of ZFAS1 has been reported to play a pivotal role in various disorders. For example, exosomal ZFAS1 has been demonstrated to facilitate gastric cancer progression [16]. To date, whether BMSC-Exos can alleviate pulmonary I/R injury via transferring ZFAS1 remains unclear and deserves further investigation.

A growing body of research has illustrated that lncRNAs post-transcriptionally modulate gene expression via interacting with RNA-binding proteins (RBPs) to mediate mRNA decay. For example, lncRNA maternally expressed gene 3 interacted with polypyrimidine tract-binding protein 1 (PTBP1) to induce Shp mRNA decay, which caused cholestatic liver injury [17]. Up-frameshift 1 (UPF1) has been identified as a key modulator of RNA decay [18]. Forkhead box D1 (FOXD1), a transcription factor, has been reported to drive the progression of lung cancer via interacting with galectin-3 (Gal-3) [19]. Nevertheless, the functional role of the FOXD1/Gal-3 axis in pulmonary I/R injury has not been documented. Interestingly, the Starbase database (https://starbase.sysu.edu.cn/index.php) has predicted that ZFAS1 and FOXD1 could bind to UPF1. Thus, we hypothesized that MSC-derived exosomal ZFAS1 reduced FOXD1 mRNA stability via interacting with UPF1 and subsequently inactivated Gal-3, thereby conferring protection against pulmonary I/R injury.

In this work, we found that BMSC-derived exosomes mitigated pulmonary I/R injury via delivering ZFAS1. Mechanistically, ZFAS1 interacted with UPF1 to trigger FOXD1 mRNA decay and succeeding Gal-3 inactivation. Our findings will provide insights into the novel mechanism of exosomal ZFAS1 in pulmonary I/R injury and identify BMSC-derived exosomal ZFAS1 as an effective intervention.

Materials and Methods

Cell Culture and Identification

BMSCs were isolated from the femurs and tibias of male and female C57BL/6 mice (8 weeks old) as described previously

[20]. In brief, the bone marrow was extracted and washed with Dulbecco's modified eagle medium (DMEM, catalog number: D5796, Sigma-Aldrich, USA) several times. After filtration and centrifugation, the isolated BMSCs were maintained in DMEM supplemented with 10% fetal bovine serum (FBS, catalog number: 10100147, Gibco, USA). For the identification of BMSCs, the positive expression of CD105, CD90, and CD73 and negative expression of human leukocyte antigen DR (HLA-DR) and CD45 were validated using flow cytometry. A pool of BMSCs from different mice was constructed and used in this study. HEK293 cells obtained from American Type Culture Collection (USA) were maintained in DMEM/F12 (catalog number: D0697, Sigma-Aldrich) with 10% FBS and placed in a humidified incubator with 5% CO_2.

Exosome Isolation and Quantification

BMSC-Exos were extracted from the cell culture supernatant of isolated mouse BMSCs as described previously [21]. In brief, BMSCs with 80% confluency were maintained in a serum-free medium for 24 h, and then, the supernatant was obtained. After filtering through a 0.22-μm filter, the collected supernatant was centrifuged at 2000 *g* for 30 min at 4 °C, followed by ultracentrifugation at 10,000 *g* for 30 min at 4 °C to remove non-exosome vesicles and at 100,000 g for 4 h at 4 °C to pellet the exosomes. BMSC-Exos were re-suspended in ice-cold phosphate-buffered saline (PBS) and stored at − 80 °C for further experiments. BMSC-Exos were observed under a transmission electron microscope. NanoSight nanoparticle tracking analysis (NTA) was used to analyze the BMSC-Exo size. Surface antigens of exosomes (CD63, CD9, tumor susceptibility gene 101 [TSG101], and heat shock protein [Hsp70]) and endoplasmic reticulum marker (Calnexin) was assessed by Western blotting.

Isolation of Primary Mouse Lung Microvascular Endothelial Cells (LMECs) and Exposure to Hypoxia/Reoxygenation (H/R)

LMECs were isolated from male and female C57BL/6 mice (8 weeks old) in accordance with a previous study [22]. In brief, after euthanasia, the lungs were collected from mice. After removing large airways and mincing, the lung tissues were digested with 1 mg/mL of collagenase (catalog number: COLLDISP-RO, Sigma-Aldrich). The digested cells were filtered, centrifugated, and maintained in DMEM containing 20% FBS, 150 μg/mL of endothelial cell growth supplement (catalog number: 211F-GS, Sigma-Aldrich), and 100 μg/mL of penicillin/streptomycin (catalog number: V900929, Sigma-Aldrich). We constructed a pool of LMECs from different mice. LMECs between passages 2 and 10 were adopted in this study. LMECs were exposed to H/R to mimic the pulmonary I/R injury in vitro. Hence, LMECs were maintained in a hypoxic chamber containing 95% N_2-5% CO_2 for 3 h, followed by culture in a normoxic chamber for 1 h [23].

PKH-26 Staining

In evaluating the uptake of BMSC-Exos by LMECs, BMSC-Exos were stained with PKH-26 (catalog number: MINI26-1KT, Sigma-Aldrich) and then added to LMECs. After incubation for 24 h, the nuclei were stained with 4′-6-diamidino-2-phenylindole (DAPI, catalog number: D9542, Sigma-Aldrich) and observed under a fluorescence microscope (Olympus, Tokyo, Japan) at a magnification of 400×.

Lentivirus Infection

Lentiviruses carrying negative control shRNA (shNC), sh-ZFAS1 (gene ID: NR_138563.1), sh-FOXD1 (gene ID: NM_008242.2), sh-UPF1 (gene ID: NM_001122829.2), sh-Gal-3 (gene ID: NM_001145953.1), and genes for ZFAS1, FOXD1, and Gal-3 were provided by GeneChem (Shanghai, China). The sequences for shRNAs were as follows: sh-ZFAS1, 5′-GGTTAACTTGCAGATGGTTGA-3′; sh-FOXD1, 5′-CGTATATCGCGCTCATCACTA-3′; sh-UPF1, 5′-GGAGTCACAGACTCAAGATAA-3′; sh-Gal-3, 5′-GCA GTACAACCATCGGATGAA-3′. BMSCs were infected with lentiviruses carrying shNC, sh-ZFAS1, or genes for ZFAS1. On the contrary, LMECs were infected with lentiviruses carrying shNC, sh-FOXD1, sh-UPF1, sh-Gal-3, and genes for FOXD1. Moreover, Gal-3 was supplemented with 5 μg/mL of polybrene (catalog number: TR-1003-G, Sigma-Aldrich). After infection for 48 h, the infected GFP-positive cells were observed under a fluorescent microscope and selected using 15 μg/mL of puromycin (catalog number: 60209ES, Yeasen, Shanghai, China).

Quantitative Real-Time PCR (qRT-PCR)

Total RNA was isolated from lung tissues or LMECs using a Trizol reagent (catalog number: 15596018, Thermo Fisher). Complementary DNA was synthesized using the Hifair® II 1st-strand cDNA synthesis kit (catalog number: 11119ES60, Yeasen). Quantitative PCR was performed using the Hieff® qPCR SYBR Green Master Mix (catalog number: 11201ES03. Yeasen). Gene expression normalized to GAPDH was calculated using the $2^{-\Delta\Delta Ct}$ method. The primer sequences are listed in Table 1. The experiment was repeated three times.

Western Blotting

Total proteins were extracted using the RIPA buffer (catalog number: 89901, Thermo Fisher), and protein concentration was determined using the BCA protein quantification kit (catalog number: 20201ES76. Yeasen). Protein samples (30 μg) were separated by 10% sodium dodecyl sulfate polyacrylamide gel electrophoresis and then transferred to polyvinylidenedifluoride membranes. The membranes were blocked with 1% bovine serum albumin and probed with primary antibodies against Calnexin (1:1000, ab133615, Abcam, UK), CD63 (1:1000, ab217345, Abcam), CD9 (1:1000, 98,327, CST, USA), TSG101 (1:1000, ab125011, Abcam), HSP70 (1:1000, 4872, CST), FOXD1 (1:500, bs-12193R, Bioss, Beijing, China), Gal-3 (1:1000, ab76245, Abcam), UPF1 (1:1000, 12,040, CST), and GAPDH (1:2500, ab8245, Abcam) at 4 °C overnight. After incubation with a peroxidase-conjugated secondary antibody, the protein bands were detected by enhanced chemiluminescence (catalog number: 32106, Pierce, USA). The experiment was repeated three times.

Cell Viability Detection

LMEC viability was assessed using the cell counting kit 8 (CCK-8, catalog number: 40203ES60, Yeasen). LMECs from different treatment groups were plated into 96-well plates at a density of 3000 cells per well and then reacted with CCK-8 solution (10 μL) for 3 h at 37 °C. The results were detected at 450 nm on a microplate reader (Tecan, Switzerland). The experiment was repeated three times.

Table 1 Oligonucleotide primer sets for qRT-PCR

Name	Sequence (5′¬3′)	Length
TNF-α F	CACAAGATGCTGGGACAGTGA	21
TNF-α R	TCCTTGATGGTGGTGCATGA	20
IL-1β F	GTTGACGGACCCCAAAAGAT	20
IL-1β R	CCTCATCCTGGAAGGTCCAC	20
IL-6 F	ACAAAGCCAGAGTCCTTCAGA	21
IL-6 R	TCCTTAGCCACTCCTTCTGT	20
ZFAS1 F	AGCGTTTGCTTTGTTCCC	18
ZFAS1 R	CTCCCTCGATGCCCTTCT	18
FOXD1 F	ACTCAGCCCTGGCCTTGC	18
FOXD1 R	GCGGGAGGAGTGAGAATCTAGAA	23
UPF1 F	AATGCAAGGAAGTGACGCTG	20
UPF1 R	AAAGCACCGGTCCTGGATTA	20
Gal-3 F	GCTACTGGCCCCTTTGGT	18
Gal-3 R	CCAGGCAAGGGCATATCGTA	20
GAPDH F	CGGCCGCATCTTCTTGTG	18
GAPDH R	CCGACCTTCACCATTTTGTCTAC	23

5-Ethynyl-2′-Deoxyuridine (EdU) Staining

EdU staining was performed to measure the proliferation of LMECs using the EdU Apollo567 in vitro kit (catalog number: CA1170, Solarbio, Beijing, China). In brief, LMECs were labeled with 50 μM of EdU solution for 2 h. After fixation in 4% formaldehyde (catalog number: F8775, Sigma-Aldrich), LMECs were added with 2 mg/mL of glycine (catalog number: G7126, Sigma-Aldrich), followed by incubation with Apollo staining buffer. Subsequently, LMECs were treated with 0.5% TritonX-100 (catalog number: T8787, Sigma-Aldrich) and stained with DAPI (catalog number: D9542, Sigma-Aldrich). Images were captured using a fluorescence microscope (Olympus, Tokyo, Japan) at a magnification of 100×. The experiment was repeated three times.

Cell apoptosis assay

LMEC apoptosis was measured using the Annexin V-FITC apoptosis detection kit (catalog number: CA1020, Solarbio). The collected LMECs were stained with 5 μL of Annexin V/FITC for 5 min in the dark and then with 5 μL PI solution. Finally, the samples were immediately analyzed using flow cytometry. The experiment was repeated three times.

Scratch Assay

LMECs were plated in six-well plates. After reaching 100% confluence, a scratch with an equal width was generated using a pipette tip. LMECs were maintained in a serum-free medium for 24 h. After the scratch, the images were captured at 0 and 24 h using a light microscope at a magnification of 100×. The experiment was repeated three times.

RNA Pull-Down

The biotinylated ZFAS1 probe and Oligo probe were purchased from RiboBio (Guangzhou, China) and added to the prepared protein extract, followed by incubation with streptavidin-labeled magnetic beads to separate RNA–protein complexes. After elution, the retrieved UPF1 protein bound to ZFAS1 was measured by Western blotting. The experiment was repeated three times.

RNA Immunoprecipitation (RIP) Assay

The interaction between UPF1 and ZFAS1/FOXD1 was validated by RIP assay using the Magna RIP™

RNA-binding protein immunoprecipitation kit (catalog number: 17–700, Millipore, USA). LMEC lysates were incubated with magnetic beads conjugated with anti-UPF1 (12,040, Cell Signaling Technology) or anti-IgG (negative control, #3900, Cell Signaling Technology) antibodies. The levels of ZFAS1 or FOXD1 in co-precipitated RNAs were assessed by qRT-PCR. The experiment was repeated three times.

Chromatin Immunoprecipitation (ChIP)

The direct binding of FOXD1 to Gal-3 promotor (binding sequences: ATAAACAT) was validated by ChIP using the ChIP assay kit (catalog number: P2078, Beyotime, Haimen, China). In brief, LMECs were cross-linked with formaldehyde and subjected to ultrasonication to produce 200–1000 bp DNA fragments. Afterward, 50 μg of DNA fragments was immunoprecipitated with protein A/G beads conjugated with anti-FOXD1 (sc-293238, Santa Cruz, USA) or anti-IgG (#3900, Cell Signaling Technology) antibodies. The immunoprecipitated DNAs were extracted, purified, and detected by DNA agarose electrophoresis. The experiment was repeated three times.

Dual-Luciferase Reporter Assay

Gal-3 promoter sequences containing FOXD1-binding sites were inserted into a pGL3 vector (catalog number: E1751 Promega, USA). HEK293 cells were transfected with the pGL3-Gal-3 plasmid and sh-FOXD1/shnc or FOXD1 overexpression plasmid/vector using Lipofectamine 2000 (catalog number: 11668019, Thermo Fisher) according to the manufacturer's instructions. After incubation for 24 h, the HEK293 cells were measured using the dual-luciferase reporter assay system (catalog number: E1910, Promega). The experiment was repeated three times.

Animal Models

Male C57BL/6 mice (8–10 weeks old) were obtained from SLAC Jingda Laboratory Animal Co., Ltd. (Hunan, China), and randomly divided into the following experimental groups ($n = 6$ per group): sham, I/R, I/R + PBS, I/R + MSC-Exos, I/R + Exos-shNC, I/R + Exos-shZFAS1, I/R + Exos-shZFAS1 + shNC, I/R + Exos-shZFAS1 + shFOXD1, and I/R + Exos-shZFAS1 + sh-Gal-3. Pulmonary I/R injury was induced in mice as previously reported [24]. All mice

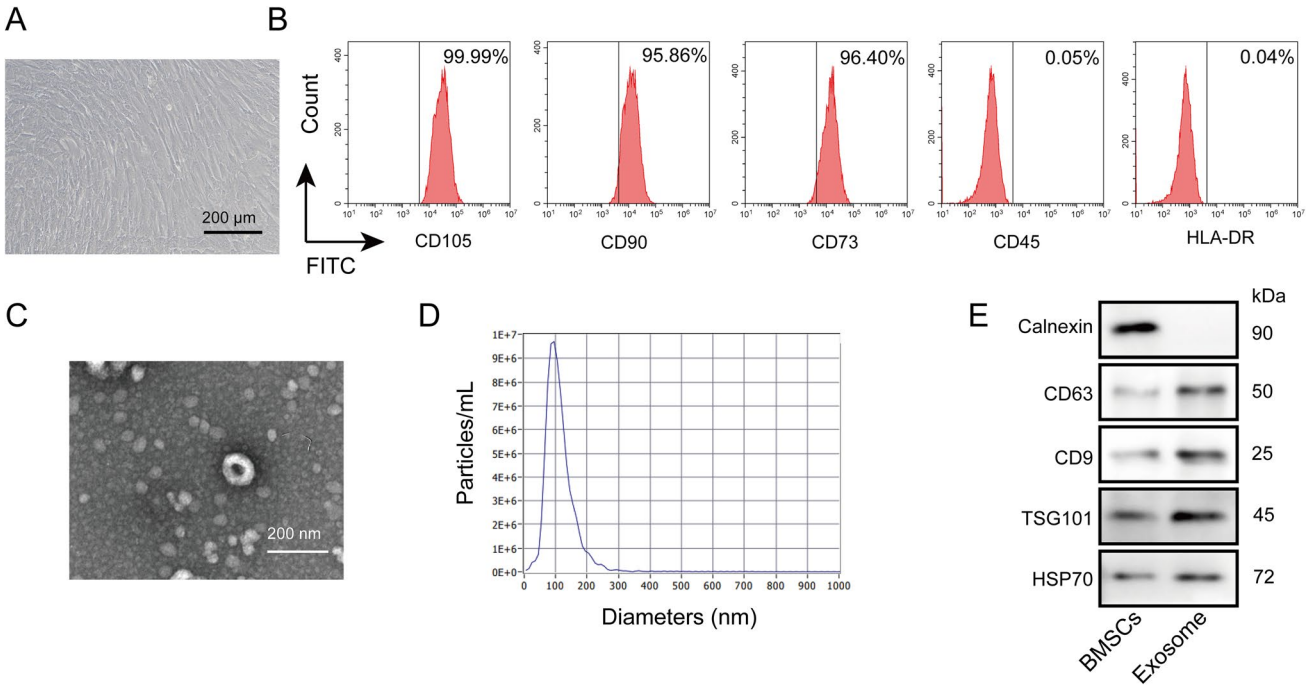

Fig. 1 Exosomes were isolated from BMSCs and identified. **A** The morphology of BMSCs was observed. Scale bars, 200 μm. **B** The expression of CD105, CD90, CD73, HLA-DR, and CD45 in BMSCs was assayed via flow cytometry. **C** Transmission electron microscopy image of exosomes isolated from BMSCs (BMSC-Exos). Scale bars, 200 μm. **D** The particle size of BMSC-Exos was analyzed by NanoSight NTA technology. **E** Markers for exosomes and the endoplasmic reticulum were analyzed by Western blotting

were subjected to anesthesia via intraperitoneal injection of 60 mg/kg pentobarbital sodium and then left anterolateral thoracotomy. The left pulmonary hilum of mice in I/R groups was blocked using a microvascular clamp for 1 h, and then, reperfusion was performed for 2 h by removing the clamp. The same operation procedure was performed in sham mice without blocking the left pulmonary hilum. Exosomes were administered to mice through intratracheal instillation in 30 μL of PBS at 24 h before the operation. Lentiviruses containing shFOXD1, sh-Gal-3, or shNC (1×10^8 PFUs in 30 μL of PBS, GeneChem) were administered via intratracheal instillation 1 week before the induction of pulmonary I/R injury. Heating pads were placed on mice during experimental procedures to maintain body temperature. The lungs were harvested from mice that were euthanatized by overdose of sodium pentobarbital. All experimental procedures were approved by the Animal Care and Use Committee of the Third Affiliated Hospital of Soochow University.

Lung Wet/Dry (W/D) Weight Ratio

The collected lungs were immediately weighed to obtain the wet weight. After drying for 2 days at 80 °C, the dry weight was measured. Finally, the W/D weight ratio was calculated.

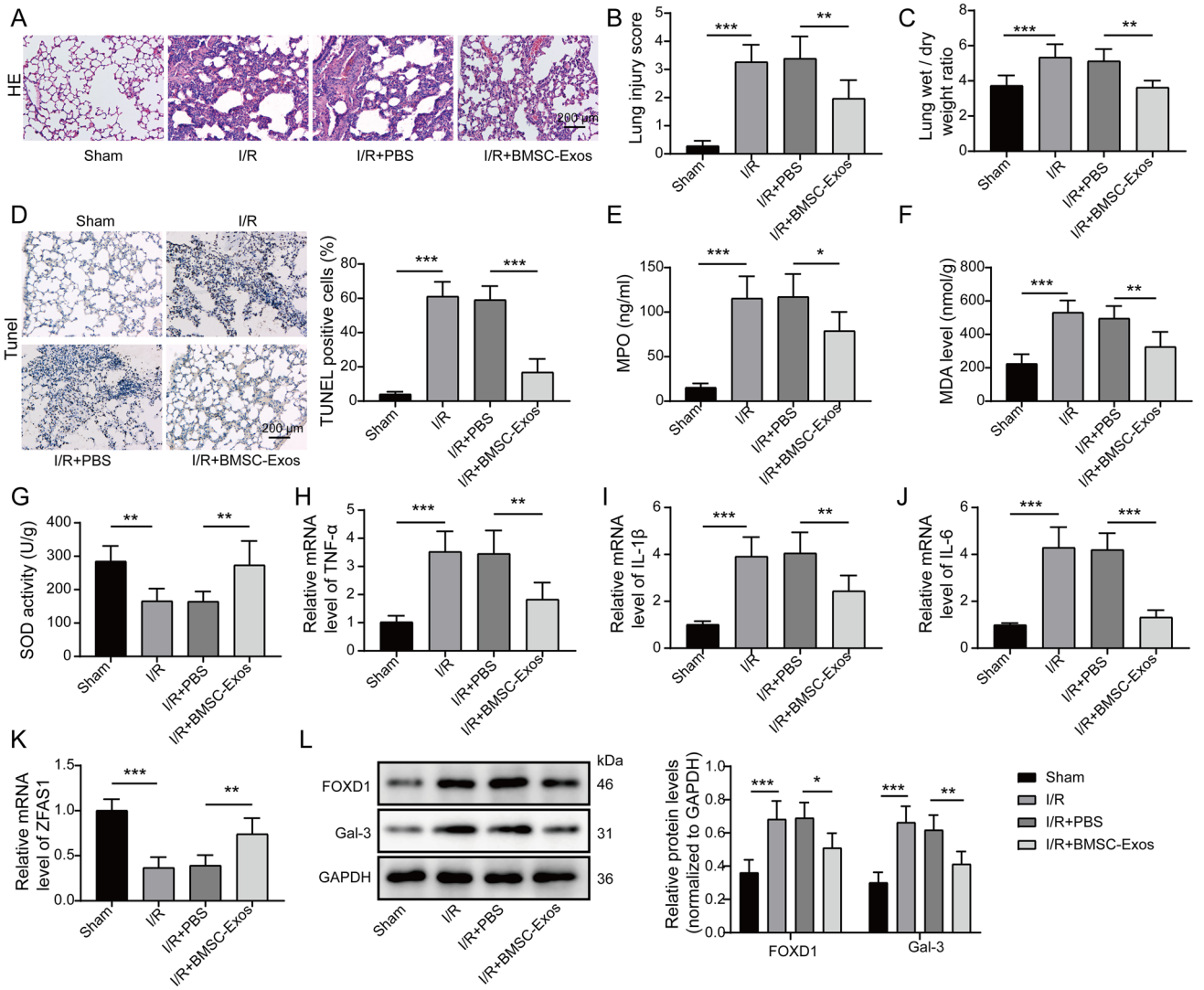

Fig. 2 BMSC-Exos protective mechanism against mouse pulmonary I/R injury in vivo. BMSC-Exos were administered to mice with pulmonary I/R injury via intratracheal instillation. **A** Lung sections were subjected to H&E staining, and histopathological changes were observed. Scale bars, 200 μm. **B** The severity of lung injury was assessed on the basis of the injury score. **C** Lung W/D weight ratio was calculated. **D** TUNEL assay was performed to determine apoptosis in lungs. Scale bars, 200 μm. **E** MPO activity, **F** MDA level, and **G** SOD activity in lung tissues were detected. **H**–**J** qRT-PCR analysis of TNF-α, IL-1β, and IL-6 expression levels in the lungs (normalized to GAPDH). **K** ZFAS1 level in lung tissues (normalized to GAPDH) was measured by qRT-PCR. **L** Western blotting analysis of FOXD1 and Gal-3 protein levels in the lungs (normalized to GAPDH expression). $n = 6$ for each data set. $^*P < 0.05$, $^{**}P < 0.01$, and $^{***}P < 0.001$

Hematoxylin and Eosin (H&E) Staining

The collected lungs of mice were fixed in 4% paraformaldehyde, followed by paraffin embedding and cutting into 5-μm slices. H&E staining was performed using a commercial HE staining kit (catalog number: AR1180-100, Boster, Wuhan, China) following the protocol. The severity of lung injury was evaluated on the basis of the injury scores as previously described [25].

Measurement of Myeloperoxidase (MPO), Superoxide Dismutase (SOD), and Malondialdehyde (MDA) Levels

The activities of MPO, SOD, and MDA in lung tissues were assessed using the mouse myeloperoxidase ELISA kit (ab275109, Abcam), the superoxide dismutase activity assay kit (ab65354, Abcam), and the lipid peroxidation (MDA)

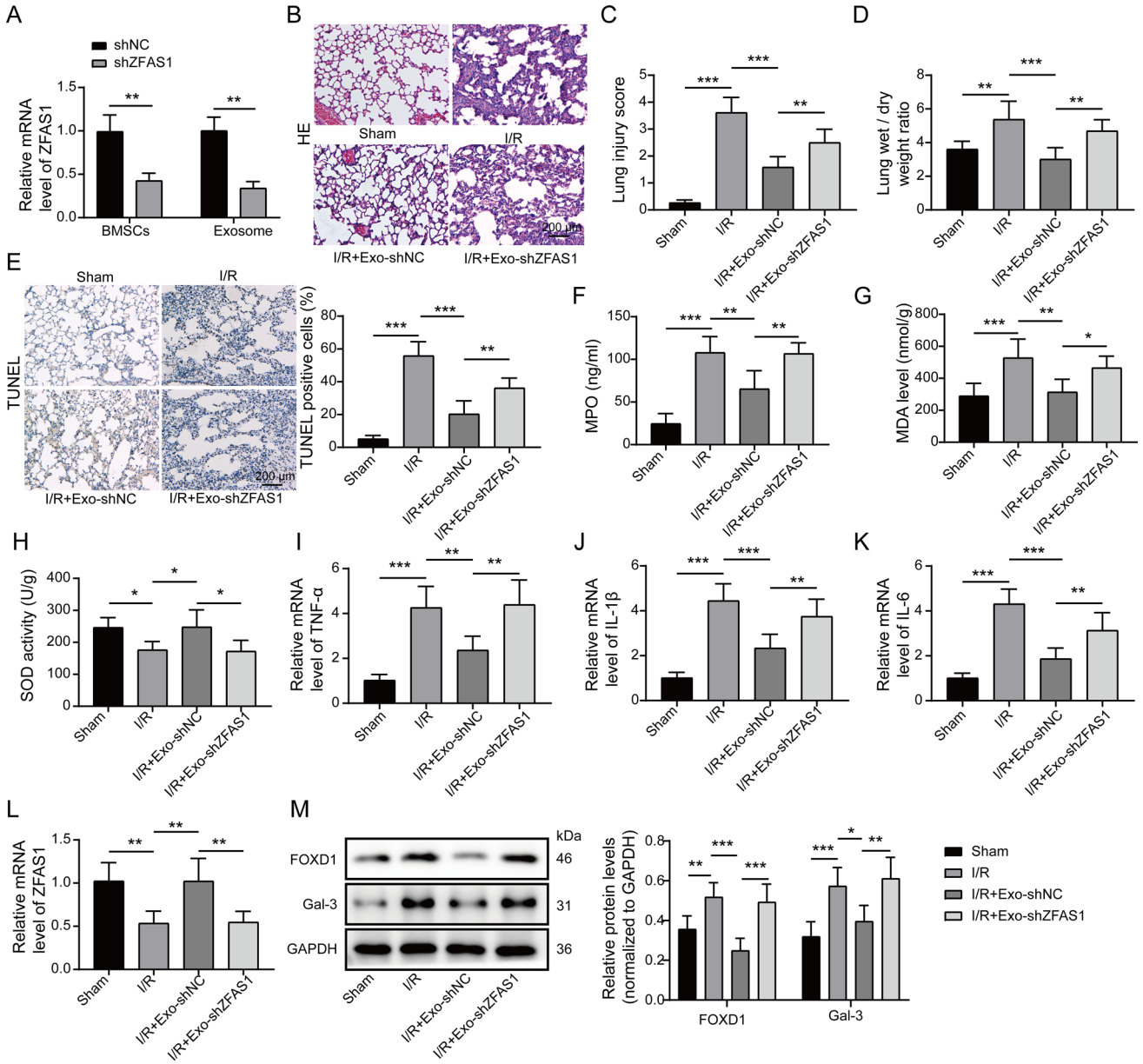

Fig. 3 BMSC-Exos carried ZFAS1 to alleviate pulmonary I/R injury. The mice with pulmonary I/R injury were treated with exosomes derived from BMSCs infected with lentiviruses carrying shNC or shZFAS1 via intratracheal instillation. **A** ZFAS1 level in BMSCs and BMSC-Exos (normalized to GAPDH) was assessed by qRT-PCR. **B** H&E staining was used to evaluate lung injury in histology. Scale bars, 200 μm. **C** Lung injury severity was determined on the basis of the injury score. **D** Lung W/D weight ratio was calculated. **E** Lung sections were subjected to TUNEL assay to detect apoptosis. Scale bars, 200 μm. **F** MPO activity, **G** MDA level, and **H** SOD activity in lung tissues were detected. **I**–**K** TNF-α, IL-1β, and IL-6 levels in the lungs (normalized to GAPDH) were assessed by qRT-PCR. **L** ZFAS1 expression in lung samples (normalized to GAPDH) was evaluated by qRT-PCR. **M** The protein abundance of FOXD1 and Gal-3 (normalized to GAPDH) in the lungs was detected by Western blotting. $n=6$ for each data set. $^{*}P<0.05$, $^{**}P<0.01$, and $^{***}P<0.001$

assay kit (ab118970, Abcam), respectively, following the manufacturers' protocols.

Terminal Deoxynucleotidyl Transferase-Mediated dUTP Nick End-Labeling (TUNEL)

Apoptosis in lung slices was detected using the TUNEL assay kit (ab206386, Abcam). In brief, the slices were permeabilized using the proteinase K solution (catalog number: 1.07393, Sigma-Aldrich) for 20 min and blocked in 3% H_2O (catalog number: W4502, Sigma-Aldrich), followed by incubation with TdT labeling reaction mix for 90 min. After incubation with stop buffer for 15 min, the slices were developed using DAB solution. Finally, the slices were observed under a light microscope (Olympus, Tokyo, Japan) at a magnification of 100×.

Statistical Analysis

Data were collected from at least three independent experiments and expressed as mean ± standard deviation. Statistical analysis was performed using SPSS17.0. Differences were tested using Student's *t*-test for two groups or one-way analysis of variance (ANOVA), followed by log-rank test for more than two groups. $P < 0.05$ was considered statistical significant.

Results

Characterization of BMSCs and Their Exosomes

Under a light microscope, we observed that mouse BMSCs were spindle shaped (Fig. 1A). In addition, the expression levels of cell surface antigens were assessed by flow cytometry. CD105, CD90, and CD73 showed a positive expression, whereas HLA-DR and CD45 showed a negative expression (Fig. 1B), thereby indicating the successful isolation of BMSCs. Subsequently, exosomes were isolated from mouse BMSCs and characterized using a transmission electron microscope. As shown in Fig. 1C, the extracted exosomes show a round or cup-like shape (Fig. 1C). NTA technology indicated that the diameter of isolated exosomes was 30–150 nM (Fig. 1D). Moreover, the positive expression of CD63, CD9, TSG101, and HSP70 and the negative expression of Calnexin in exosomes were validated by Western blotting (Fig. 1E). Therefore, exosomes were successfully extracted from mouse BMSCs.

BMSC-Derived Exosomes Relieve Pulmonary I/R Injury in Mice

In determining whether BMSC-Exos could attenuate pulmonary I/R injury, mice were administered with BMSC-Exos 24 h before lung I/R injury. We found that all mice survived after pulmonary I/R injury. Treatment with BMSC-Exos alleviated the I/R injury-induced disorder structure of pulmonary tissue and inflammatory infiltration (Fig. 2A). The enhanced lung injury score in the pulmonary I/R injury group was reduced after administration of BMSC-Exos (Fig. 2B). In addition, pulmonary edema as evidenced by an increase in lung W/D weight ratio in mice with pulmonary I/R injury was weakened by BMSC-Exo treatment (Fig. 2C). Moreover, apoptosis was triggered by pulmonary I/R injury in lung tissues, but BMSC-Exo treatment effectively restrained apoptosis (Fig. 2D). Furthermore, I/R injury significantly increased MPO and MDA levels but reduced SOD activity in the lungs, which were reversed by the delivery of BMSC-Exos (Fig. 2E–G). We also observed amplified lung inflammation in the I/R group based on the upregulation of TNF-α, IL-1β, and IL-6. However, the administration of BMSC-Exos effectively reduced the levels of these pro-inflammatory cytokines (Fig. 2H–J). Interestingly, the ZFAS1 level was reduced, whereas FOXD1 and Gal-3 levels were increased in the lungs in response to lung I/R stimulation. On the contrary, these changes were reversed after treatment with BMSC-Exos (Fig. 2K–L). These observations indicated that BMSC-Exos relieved pulmonary I/R injury

Fig. 4 BMSC-Exos restrained H/R-induced proliferation and migration inhibition and apoptosis of LMECs via carrying ZFAS1. **A** ZFAS1 expression level in BMSCs and BMSC-Exos (normalized to GAPDH) was detected by qRT-PCR. **B** BMSC-Exos were labeled with PKH-26 and co-cultured with LMECs for 24 h. After nuclear staining with DAPI, LMECs were observed under a fluorescence microscope. Scale bars, 20 μm. **C** LMECs were exposed to H/R with or without treatment with exosomes derived from BMSCs infected with lentiviruses carrying shNC, shZFAS1, vector, or ZFAS1. The ZFAS1 level (normalized to GAPDH) in LMECs from various groups was measured by qRT-PCR. The proliferation of LMECs was assessed by CCK-8 (**D**) and EdU staining (**E**). Scale bars, 200 μm. **F** The apoptotic rate of LMECs with different treatments was determined by flow cytometry. **G** The migratory capacity of LMECs was detected by Scratch assay. Scale bars, 500 μm. **H–J** TNF-α, IL-1β, and IL-6 levels in LMECs (normalized to GAPDH) were measured by qRT-PCR. **K** Western blotting analysis of the protein abundance of FOXD1 and Gal-3 in LMECs (normalized to GAPDH). $n = 3$ for each data set. $^*P < 0.05$, $^{**}P < 0.01$, and $^{***}P < 0.001$

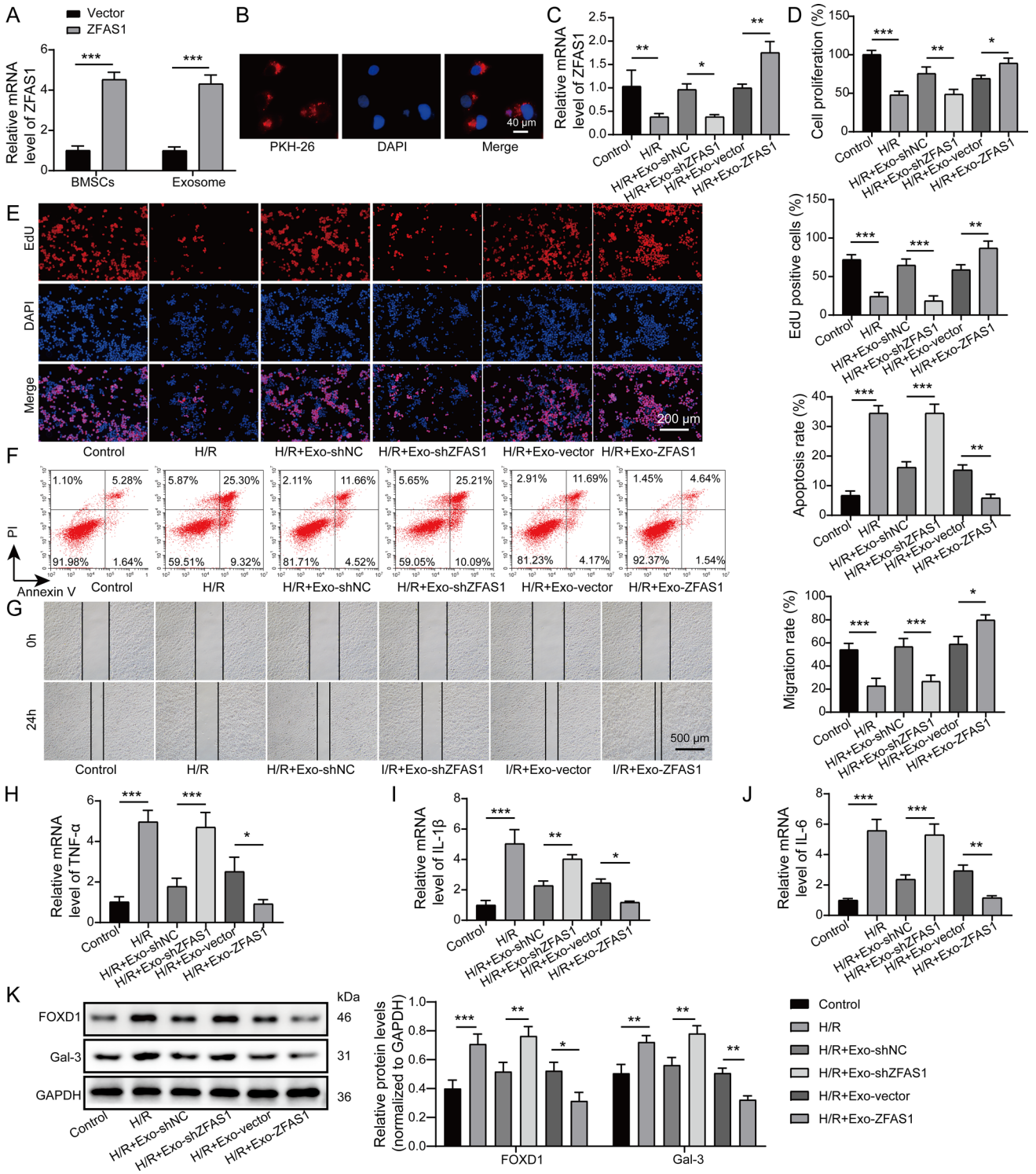
A
Vector
ZFAS1
Relative mRNA level of ZFAS1
BMSCs
Exosome
B
PKH-26
DAPI
Merge
40 μm
C
Relative mRNA level of ZFAS1
D
Cell proliferation (%)
E
EdU
DAPI
Merge
200 μm
EdU positive cells (%)
F
PI
Annexin V
1.10% 5.28% 91.98% 1.64%
5.87% 25.30% 59.51% 9.32%
2.11% 11.66% 81.71% 4.52%
5.65% 25.21% 59.05% 10.09%
2.91% 11.69% 81.23% 4.17%
1.45% 4.64% 92.37% 1.54%
Apoptosis rate (%)
G
0h
24h
500 μm
Migration rate (%)
Control
H/R
H/R+Exo-shNC
H/R+Exo-shZFAS1
H/R+Exo-vector
H/R+Exo-ZFAS1
I/R+Exo-shZFAS1
I/R+Exo-vector
I/R+Exo-ZFAS1
H
Relative mRNA level of TNF-α
I
Relative mRNA level of IL-1β
J
Relative mRNA level of IL-6
K
FOXD1
Gal-3
GAPDH
kDa
46
31
36
Relative protein levels (normalized to GAPDH)

in mice, and ZFAS1, FOXD1, and Gal-3 might be involved in the beneficial effect mechanism of BMSC-Exos.

BMSC-Derived Exosomes Induce Protection Against Pulmonary I/R Injury via Delivering lncRNA ZFAS1

Given that BMSC-Exos enhanced ZFAS1 expression in a pulmonary I/R injury model, we further explored the role of ZFAS1 in BMSC-Exos-mediated protection against pulmonary I/R injury. Thus, exosomes were isolated from BMSCs infected with lentiviruses carrying shZFAS1 or shNC. The silencing efficiency of ZFAS1 in BMSCs and BMSC-Exos was validated by qRT-PCR (Fig. 3A). H&E staining showed that BMSC-Exos-mediated attenuation in pathological changes of lung tissues was counteracted by exosomal ZFAS1 silencing (Fig. 3B and C). Moreover, compared with the BMSC-Exos-shNC group, the lung W/D weight ratio in the BMSC-Exos-shZFAS1 group was remarkably higher (Fig. 3D). The inhibitory effect of BMSC-Exos on apoptosis in lung tissues could be abolished by the knockdown of ZFAS1 in BMSC-Exos (Fig. 3E). Furthermore, the depletion of ZFAS1 in BMSC-Exos reversed the reduced MPO and MDA levels and increased SOD activity in BMSC-Exos-treated lung tissues (Fig. 3F–H). In addition, BMSC-Exos-induced inhibition in inflammatory cytokine release could be abrogated when BMSC-Exos-derived exosomal ZFAS1 was silenced (Fig. 3I–K). The high expression of ZFAS1 and low expression of FOXD1 and Gal-3 in the lungs of the BMSC-Exos-shNC group could be reversed in the BMSC-Exos-shZFAS1 group (Fig. 3L and M). Collectively, these results indicated that BMSC-Exos relieved pulmonary I/R injury via transferring ZFAS1.

BMSC-Derived Exosomal ZFAS1 Regulates the Proliferation, Apoptosis, and Migration of LMECs

In validating the protective effects of BMSC-derived exosomal ZFAS1 in vitro, LMECs were exposed to H/R to simulate pulmonary I/R injury. The overexpression efficiency of ZFAS1 in BMSCs and BMSC-Exos was confirmed by qRT-PCR (Fig. 4A). Exosomes were isolated from BMSCs infected with lentiviruses carrying shZFAS1, shNC, vector, or ZFAS1. After incubation with BMSC-Exos, the uptake of PKH26-labeled exosomes by LMECs was observed (Fig. 4B). In line with the in vivo data, ZFAS1 was downregulated in H/R-stimulated LMECs. BMSC-Exo treatment significantly enhanced ZFAS1 expression in H/R-exposed LMECs, which was counteracted by silencing of exosomal ZFAS1 but reinforced by the overexpression of exosomal ZFAS1 (Fig. 4C). Functional experiments demonstrated that H/R-induced decreased proliferation and migration capacities, and the apoptosis of LMECs could be restrained by BMSC-Exo administration (Fig. 4D–G). These BMSC-Exos-mediated changes were abolished by ZFAS1 inhibition, whereas ZFAS1 overexpression achieved opposite results (Fig. 4D–G). Similarly, BMSC-Exos repressed the release of inflammatory cytokines in H/R-exposed LMECs, which was inhibited by exosomal ZFAS1 depletion but intensified by exosomal ZFAS1 overexpression (Fig. 4H–J). Consistent with the in vivo results, FOXD1 and Gal-3 levels were increased in H/R-challenged LMECs, whereas BMSC-Exos effectively reduced the expression of these molecules (Fig. 4K). The regulatory effect of BMSC-Exos on FOXD1 and Gal-3 expression was abrogated by exosomal ZFAS1 knockdown and promoted by exosomal ZFAS1 overexpression (Fig. 4K). These results indicated that BMSC-Exos suppressed H/R-induced proliferation, migration inhibition, and apoptosis in LMECs via delivering ZFAS1.

FOXD1 Is Essential for ZFAS1-Mediated Biological Functions

Given that FOXD1 expression was modulated by BMSC-derived exosomal ZFAS1, we further investigated whether FOXD1 was involved in the biological function of exosomal ZFAS1. LMECs were infected with lentiviruses carrying shNC or shFOXD1. As shown in Fig. 5A and B, FOXD1 interference abolishes BMSC-derived exosomal ZFAS1 depletion-mediated proliferation inhibition in LMECs. In addition, the enhanced apoptosis and weakened migration of LMECs induced by ZFAS1 silencing in BMSC-Exos could be counteracted by FOXD1 suppression (Fig. 5C and D). Moreover, the downregulation of FOXD1 repressed the promotive effect of exosomal ZFAS1 depletion on inflammatory cytokine expression (Fig. 5E–G). Furthermore, the upregulation of FOXD1 and Gal-3 by exosomal ZFAS1 knockdown was reversed in FOXD1-silenced LMECs (Fig. 5H). Therefore, FOXD1 played a role in BMSC-derived exosomal ZFAS1-mediated biological functions in LMECs.

ZFAS1 Triggers the Destabilization of FOXD1 mRNA via Interacting with UPF1 in LMECs

We further explored the regulatory mechanism of ZFAS1 in FOXD1 expression in LMECs. RNA pull-down and RIP assays demonstrated a direct interaction between ZFAS1 and UPF1 in LMECs (Fig. 6A and B). Notably, UPF1 could also bind to FOXD1 based on the RIP assay (Fig. 6C). In addition, LMECs were infected with lentiviruses containing shNC or shUPF1, and we found that the depletion of UPF1 remarkably reduced UPF1 expression but increased FOXD1 expression in LMECs (Fig. 6D and E). The overexpression of ZFAS1 remarkably decreased FOXD1 expression, which was reversed by UPF1 knockdown (Fig. 6F and G). Furthermore, the interaction between UPF1 and FOXD1 in LMECs was weakened

by ZFAS1 silencing (Fig. 6H). The stability of FOXD1 mRNA was reduced in ZFAS1-overexpressed LMECs, which could be restored by co-transfection with shUPF1 (Fig. 6I). These findings indicated that ZFAS1 could cause FOXD1 mRNA decay by directly interacting with UPF1.

FOXD1 Is a Transcriptional Factor of Gal-3

Next, we focused on the downstream modulatory mechanism of FOXD1. The luciferase activity of Gal-3 was reduced by the knockdown of FOXD1, whereas the overexpression of

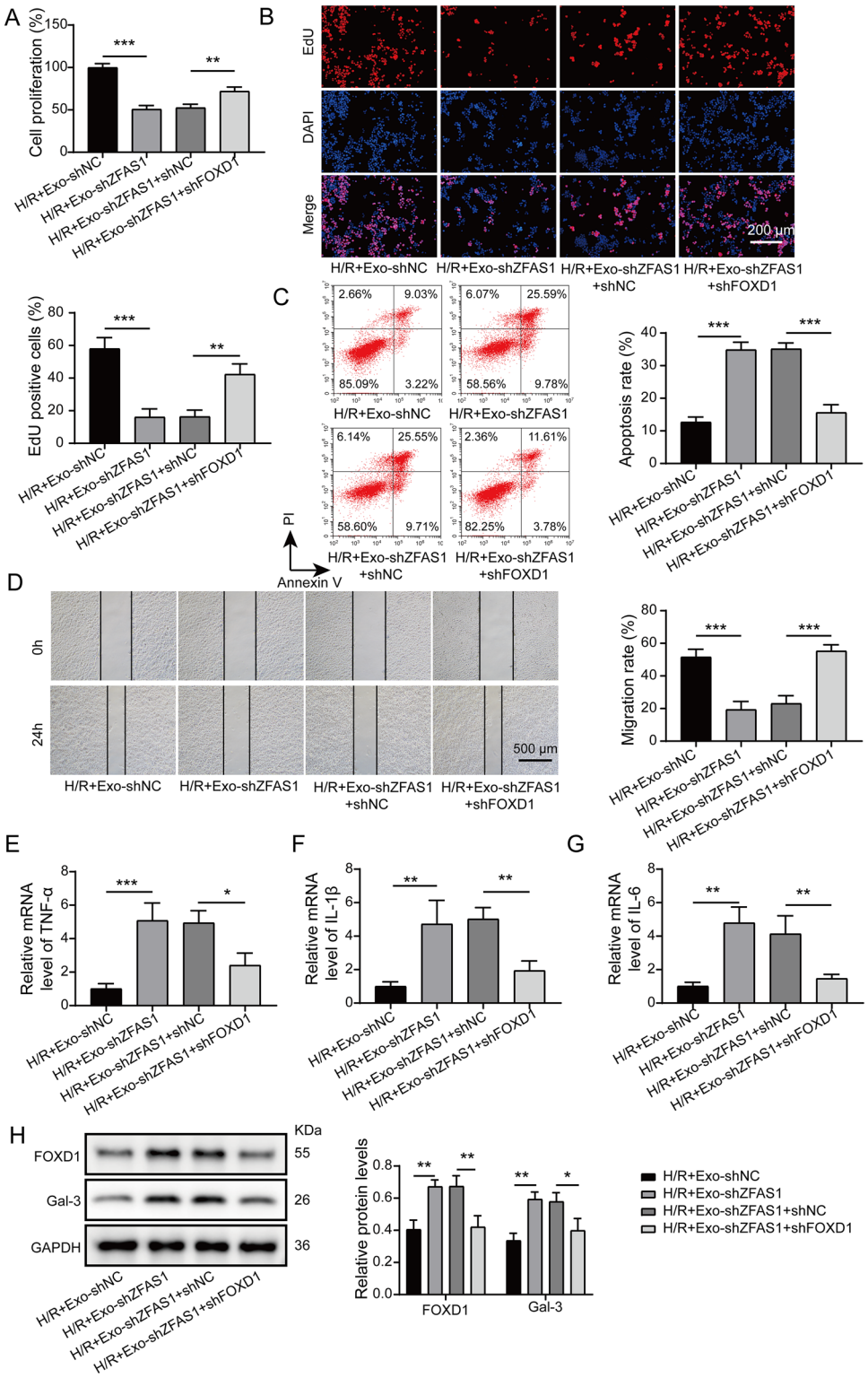

Fig. 5 FOXD1 was involved in ZFAS1-mediated biological functions in H/R-exposed LMECs. LMECs were infected with lentiviruses containing shNC or shFOXD1 and then subjected to various treatments. CCK-8 (**A**) and EdU staining (**B**) were utilized to determine the proliferation of LMECs. Scale bars, 200 μm. **C** Apoptosis of LMECs that received various treatments was assessed by flow cytometry. **D** Scratch assay was performed to evaluate LMEC migration. Scale bars, 500 μm. **E–G** qRT-PCR analysis of mRNA levels of TNF-α, IL-1β, and IL-6 in LMECs (normalized to GAPDH). **H** Western blotting analysis of protein levels of FOXD1 and Gal-3 in LMECs (normalized to GAPDH). $n = 3$ for each data set. $^{*}P < 0.05$, $^{**}P < 0.01$, and $^{***}P < 0.001$

FOXD1 showed opposite effects (Fig. 7A). The ChIP assay further validated that FOXD1 directly bound to Gal-3 promotor (Fig. 7B). Moreover, LMECs were infected with lentiviruses carrying shNC, shFOXD1, vector, or FOXD1 overexpression plasmid. The results showed that the depletion of FOXD1 downregulated Gal-3, whereas the enforced expression of FOXD1 upregulated Gal-3 in LMECs (Fig. 7C and D). Collectively, FOXD1 directly bound to Gal-3 promotor and promoted the transcription and expression of Gal-3.

Knockdown of FOXD1 Represses H/R-Induced Injury in LMECs via Inhibiting Gal-3

We further examined whether FOXD1 affected H/R-induced injury in LMECs via regulating Gal-3. LMECs were infected with lentiviruses carrying shFOXD1 with or without the Gal3 gene. As presented in Fig. 8A and B, Gal-3 mRNA and protein levels are significantly increased in LMECs after infection with lentiviruses carrying the Gal3 gene. Moreover, the proliferation and migration were facilitated, whereas apoptosis in H/R-stimulated LMECs was repressed by FOXD1 depletion; however, these FOXD1 depletion-induced changes were abrogated by Gal-3 overexpression (Fig. 8C–F). Accordingly, the inhibitory effect of FOXD1 silencing on inflammatory response was attenuated by Gal-3 overexpression (Fig. 8G–I). Collectively, the knockdown of FOXD1 induced protection against H/R-induced injury in LMECs via suppressing Gal-3 expression.

BMSC-Derived Exosomal ZFAS1 Exerts Protection Against Pulmonary I/R Injury Through Regulating the FOXD1/Gal-3 Axis

Finally, the role of the FOXD1/Gal-3 axis in the beneficial effect of BMSC-derived exosomal ZFAS1 on pulmonary I/R injury was validated in vivo. The knockdown of exosomal ZFAS1 aggravated pathological changes in the lungs of pulmonary I/R mice, whereas the inhibition of FOXD1 or Gal-3

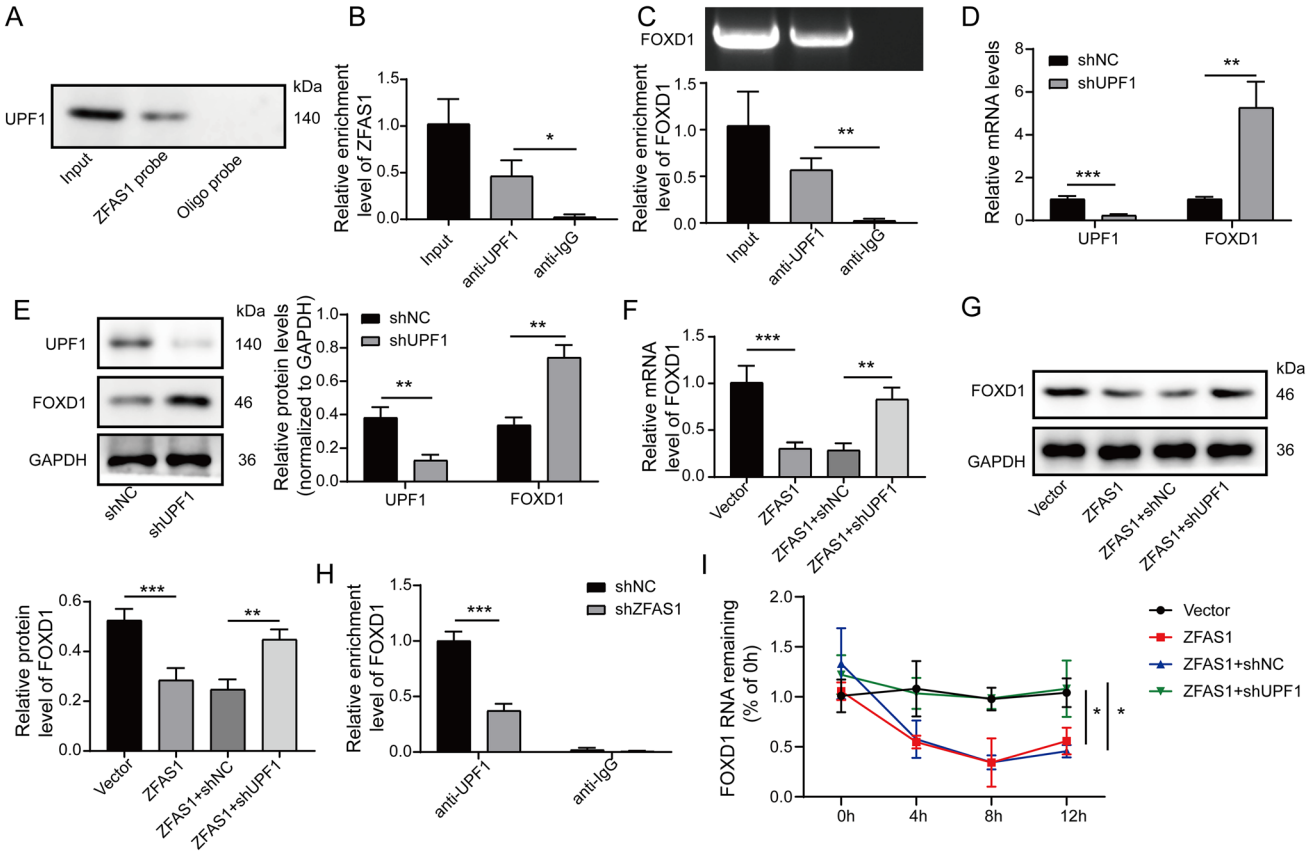

Fig. 6 ZFAS1 promoted the mRNA decay of FOXD1 via interacting with UPF1 in LMECs. **A** RNA pull-down was performed to confirm the direct binding between ZFAS1 and UPF1 in LMECs. **B** and **C** The interaction between UPF1 and ZFAS1/FOXD1 in LMECs was validated by the RIP assay. LMECs were infected with lentiviruses containing shNC or shUPF1. **D** and **F** The mRNA levels of UPF1 and FOXD1 in LMECs (normalized to GAPDH) were assessed by qRT-PCR. **E** and **G** The protein abundance of UPF1 and FOXD1 in LMECs (normalized to GAPDH) was determined by Western blotting. **H** The RIP assay was adopted to assess the interaction between UPF1 and FOXD1 in ZFAS1-silenced LMECs. **I** The stability of FOXD1 mRNA in actinomycin D-treated LMECs was evaluated. $n = 3$ for each data set. $^{*}P < 0.05$, $^{**}P < 0.01$, and $^{***}P < 0.001$

effectively attenuated lung I/R injury (Fig. 9A and B). In addition, pulmonary edema and apoptosis were promoted by exosomal ZFAS1 silencing, which were repressed after the downregulation of FOXD1 or Gal-3 in lung tissues (Fig. 9C and D). Consistently, the exosomal ZFAS1 depletion-mediated upregulation of MPO activity, MDA content, and inflammatory cytokine levels and the downregulation of SOD activity in lung tissues were all counteracted in FOXD1- or Gal-3-silenced groups (Fig. 9E–J). Western blotting showed that FOXD1 and Gal-3 levels were increased by treatment with ZFAS1-depleted BMSC-Exos; however, these changes were abolished by FOXD1 or Gal-3 knockdown (Fig. 9K). Collectively, BMSC-derived exosomal ZFAS1 relieved in vivo pulmonary I/R injury via modulating the FOXD1/Gal-3 axis.

Discussion

Pulmonary I/R injury remains a major cause of poor prognosis and high mortality after lung transplantation [26]. Therefore, developing novel effective therapeutic approaches is necessary to delay the progression of pulmonary I/R injury. Recently, BMSC-Exos have been recognized as a therapeutic option for pulmonary I/R injury [9]. However, its potential protective mechanism remains unclear; thus, more studies must be conducted. In this study, we found that lncRNA ZFAS1 delivered by BMSC-Exos alleviated pulmonary I/R injury through UPF1-mediated FOXD1 mRNA decay and subsequent inactivation of Gal-3. Our data provided insights into the molecular mechanism through which BMSC-Exos attenuated pulmonary I/R injury.

Growing evidence has indicated that MSCs derived from various tissues are conducive to tissue repair, regeneration, and inflammation inhibition through an exosome-mediated paracrine effect [27]. Functional proteins and nucleotides (including lncRNAs and miRNAs) can be carried by exosomes and then taken up by receptor cells, thereby affecting the transduction of multiple signaling pathways [28]. According to Chen et al., BMSC-Exos induced protection against myocardial I/R injury via delivering miR-125b [29]. With regard to pulmonary I/R injury, MSC-Exos played anti-inflammatory and anti-apoptotic roles in lung tissues during pulmonary I/R injury via transporting miR-21-5p [9]. Consistent with previous observations, we demonstrated that BMSC-Exo administration improved pathological changes in the lungs, edema, inflammatory response, and apoptosis in the mouse model of lung I/R injury and inhibited H/R-triggered lung epithelial cell inflammation and apoptosis in vitro. Interestingly, BMSC-Exos enhanced ZFAS1 expression in lungs, indicating that BMSC-Exos induced beneficial effects via the transportation of ZFAS1.

In addition, the inhibitory role of ZFAS1 in apoptosis and inflammation during cerebral I/R injury has been reported [30], although the influence of ZFAS1 on pulmonary I/R injury remains unknown. Notably, ZFAS1 has been documented to alleviate sepsis-induced lung injury

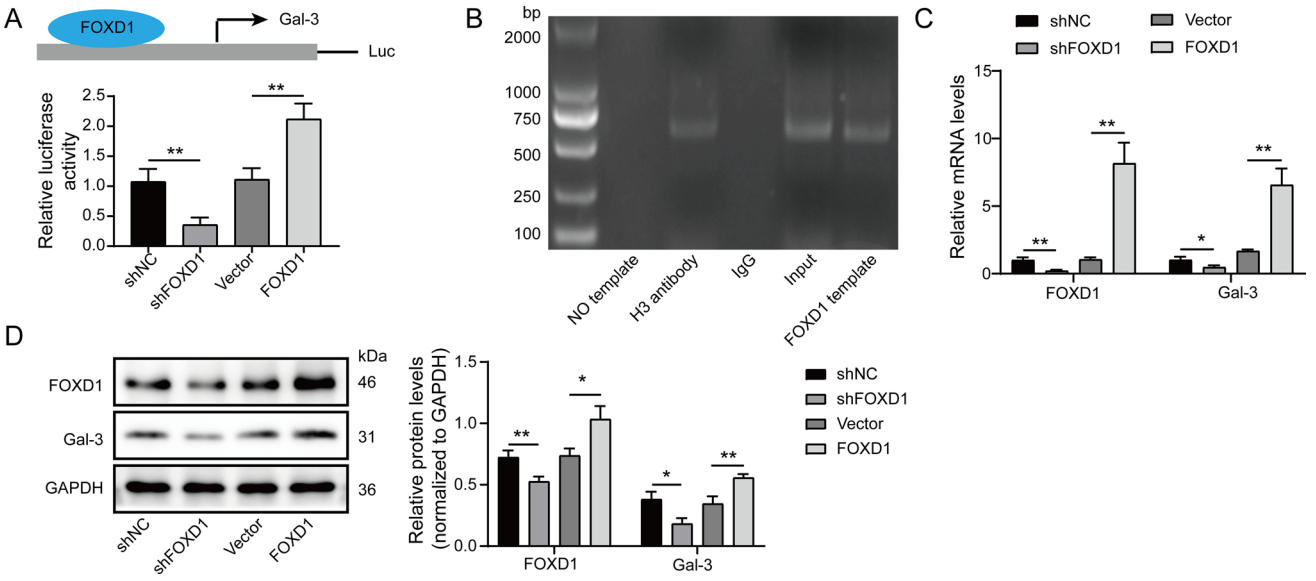

Fig. 7 FOXD1 transcriptionally regulated Gal-3 expression. **A** HEK293 cells were transfected with the pGL3-Gal-3 plasmid and sh-FOXD1/shnc or FOXD1 overexpression plasmid/vector, and the luciferase activity was detected. **B** ChIP assay analysis of the binding of FOXD1 to Gal-3 promoter in LMECs. LMECs were infected with lentiviruses carrying shNC, shFOXD1, vector, or FOXD1 overexpression plasmid. **C** and **D** FOXD1 and Gal-3 levels (normalized to GAPDH) in LMECs infected with lentiviruses carrying shNC, shFOXD1, vector, or FOXD1 overexpression plasmid were measured by qRT-PCR and Western blotting. $n=3$ for each data set. $^{*}P<0.05$, $^{**}P<0.01$ and $^{***}P<0.001$

via repressing inflammation and apoptosis [15]. In our report, silencing of exosomal ZFAS1 abrogated the beneficial effect of MSC-Exos on pulmonary I/R injury in vivo and in vitro, providing the first evidence that BMSC-Exos induced protection against pulmonary I/R injury via delivering ZFAS1.

Extensive research has suggested that lncRNAs can modulate gene transcription via interaction with RBPs [31]. As an RBP, UPF1 has been recognized as a regulator of the mRNA degradation pathway [32]. Based on previous reports, lncRNA zinc finger protein multitype 2 antisense RNA 1 (ZFPM2-AS1) interacted with UPF1 to trigger the degradation of ZFPM2, which accelerated lung adenocarcinoma progression [33]. In this work, UPF1 was considered as an RBP of ZFAS1. Further experiments revealed that ZFAS1 destabilized FOXD1 mRNA via interaction with UPF1 in LMECs. FOXD1 is a member of the forkhead box transcription factor family, which participates in

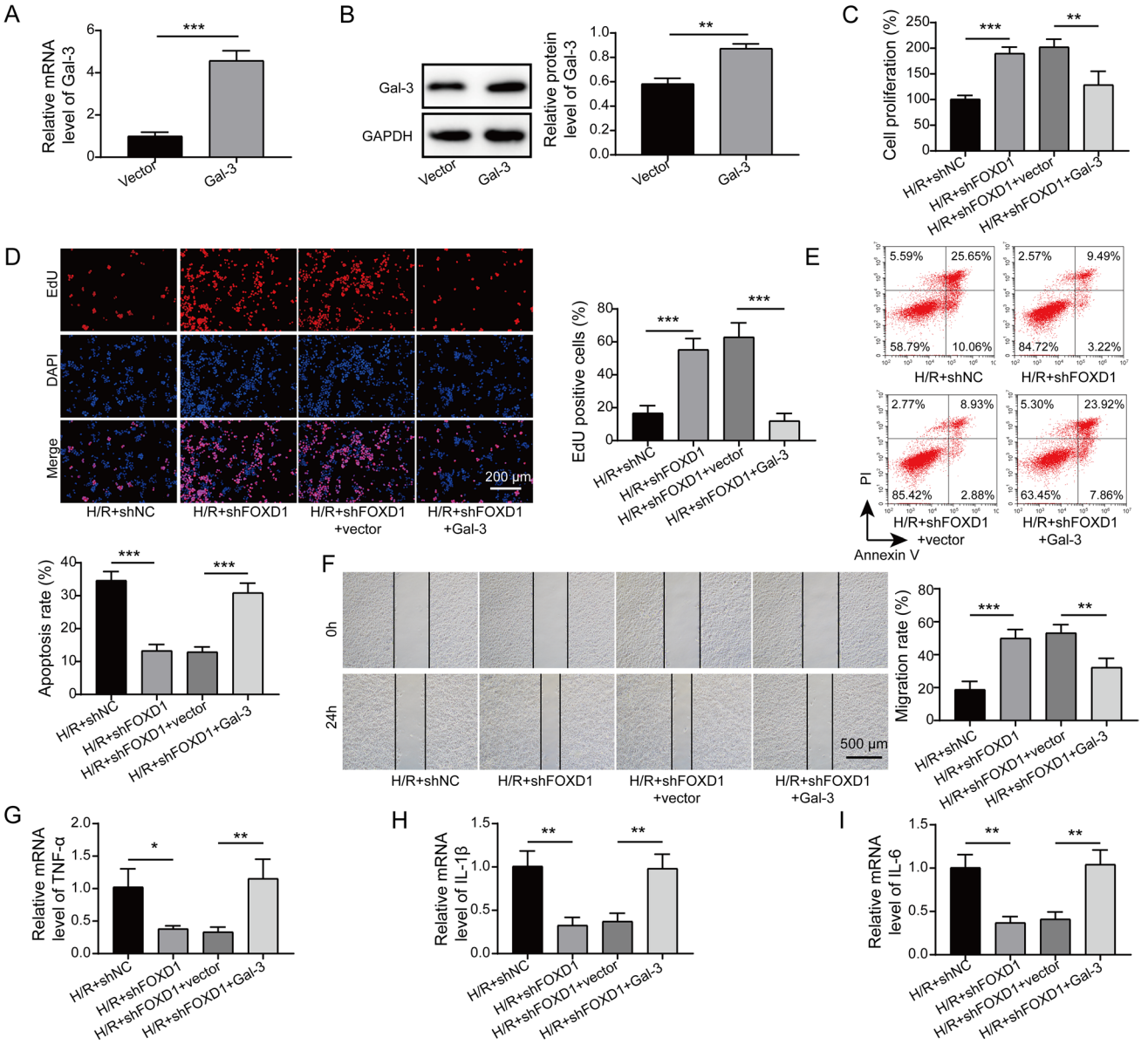

Fig. 8 FOXD1 depletion restrained H/R-induced injury in LMECs via modulating Gal-3 expression. LMECs were infected with lentiviruses carrying shFOXD1 with or without Gal3 gene and then subjected to H/R. qRT-PCR (**A**) and Western blotting (**B**) analysis of Gal-3 expression (normalized to GAPDH) in LMECs. CCK-8 (**C**) and EdU staining (**D**) were adopted to determine the proliferative ability of LMECs. Scale bars, 200 μm. **E** Apoptosis of LMECs subjected to different treatments was detected by flow cytometry. **F** LMEC migration was evaluated by Scratch assay. Scale bars, 500 μm. **G–I** qRT-PCR analysis of TNF-α, IL-1β, and IL-6 expression in LMECs (normalized to GAPDH). $n=3$ for each data set. *$P<0.05$, **$P<0.01$, and ***$P<0.001$

various pathophysiologic processes, including embryogenesis, metabolism, cell cycle, and apoptosis modulation [34]. For example, FOXD1 could affect the occurrence and progression of a variety of tumors [35, 36]. Based on a previous study, FOXD1 modulated inflammatory reactions and prevented autoimmunity via the NF-kappaB/NFAT pathway [37]. Notably, FOXD1 has been shown to play a role in renal I/R injury [38]. These observations indicated the close association of FOXD1 with inflammation and I/R injury. In the present study, the knockdown of FOXD1 reversed the promotive role of exosomal ZFAS1 downregulation in H/R-induced injury, indicating that the UPF1-mediated

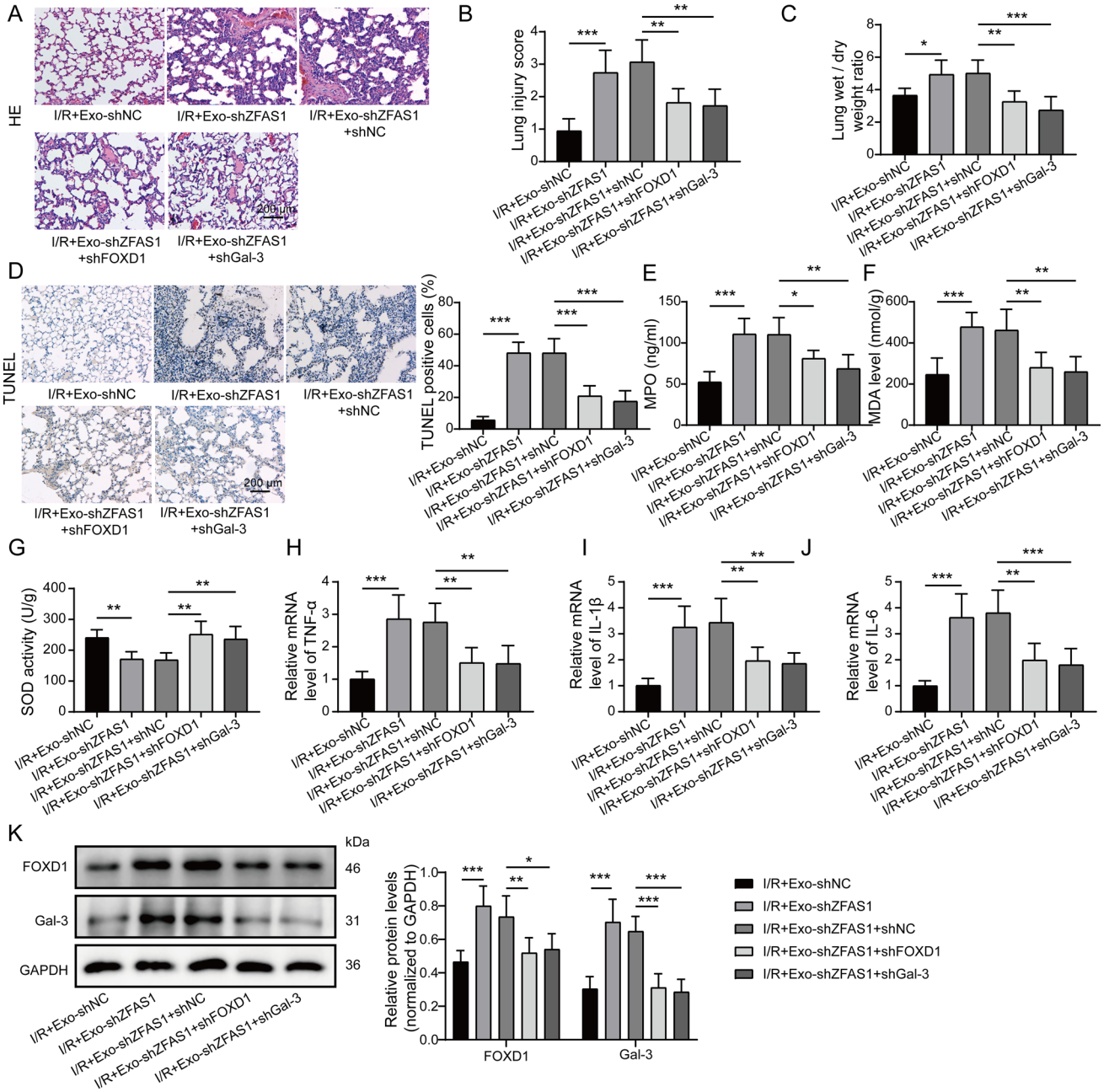

Fig. 9 FOXD1/Gal-3 axis participated in the protection of BMSC-derived exosomal ZFAS1 against pulmonary I/R injury in vivo. **A** Lung sections were subjected to H&E staining to determine histopathological changes. Scale bars, 200 μm. **B** The severity of lung injury was assessed on the basis of the injury score. **C** Lung W/D weight ratio was calculated. **D** TUNEL assay was performed to determine apoptosis in the lungs. Scale bars, 200 μm. **E** MPO activity, **F** MDA level, and **G** SOD activity in lung tissues were measured. **H–J** qRT-PCR analysis of TNF-α, IL-1β, and IL-6 mRNA levels in lung samples (normalized to GAPDH). **K** Western blotting analysis of protein abundance of FOXD1 and Gal-3 in the lungs (normalized to GAPDH). $n=6$ for each data set. $^{*}P<0.05$, $^{**}P<0.01$, and $^{***}P<0.001$

degradation of FOXD1 was involved in the beneficial mechanism of BMSC-derived exosomal ZFAS1.

Gal-3, a pleiotropic β-galactoside-binding lectin, has been considered as a master regulator of multiple biological processes, including proliferation, inflammation, apoptosis, and immunoregulation [39–41]. Based on previous reports, Gal-3 was responsible for ozone-induced lung injury via facilitating the accumulation of pro-inflammatory macrophages [42]. To date, the involvement of Gal-3 in pulmonary I/R injury has not been well-understood. According to Li et al., FOXD1 and Gal-3 reciprocally regulated each other during lung cancer development [19]. In the current work, FOXD1 bound to the Gal-3 promoter, thereby promoting the transcription and expression of Gal-3 in LMECs. The overexpression of Gal-3 hindered the beneficial effect of FOXD1 depletion on H/R-induced injury in LMECs. For the first time, these findings highlighted that the FOXD1/Gal-3 axis served as a pivotal contributor to pulmonary I/R injury.

This study had several limitations. First, intratracheal administration was applied in mice in this study. However, the implementation of endotracheal intubation in clinical practice is limited because of lack of experienced airway providers in many rural and remote settings [43]. Therefore, intratracheal administration may not be a simple and appropriate delivery route in patients. Second, we selected single administration of BMSC-Exos in mice with pulmonary I/R injury. However, the efficacy of repeated administration and the long-term efficacy of BMSC-Exos remain unclear. Thus, determining the suitable administration of BMSC-Exos must be further investigated.

Our data indicated that BMSC-derived exosomal ZFAS1 relieved pulmonary I/R injury by directly interacting with UPF1 to destabilize FOXD1 and subsequently inactivating the Gal-3 pathway, which uncovered the underlying protective mechanism of BMSC-Exos. Our results provided theoretical evidence for the application of exosomal ZFAS1 derived from BMSC-Exos in the clinical treatment of pulmonary I/R injury.

Acknowledgements We would like to give our sincere gratitude to the reviewers for their constructive comments.

Author Contribution Cao Gao: Conceptualization, Writing-original draft preparation, Investigation, Validation, Visualization, Methodology.

Yan-Jie Xu: Software.

Zhi-xiu Meng: Methodology.

Shuang Gu: Data curation.

Lei Zhang: Visualization.

Liang Zheng: Conceptualization, Writing-original draft preparation, Supervision, Writing-reviewing and editing.

Funding This work was supported in part by Changzhou HighLevel Medical Talents Training Project (KY20221373 and KY20221357) and the Major Program of Science and Technology Project of Changzhou Health Commission (ZD202206).

Availability of Data and Material All data generated or analyzed during this study are included in this published article.

Declarations

Ethics Approval and Consent to Participate The lungs were harvested after euthanasia by overdose of sodium pentobarbital. All procedures were approved by the Animal Care and Use Committee of the Third Affiliated Hospital of Soochow University.

Consent for Publication The informed consent obtained from study participants.

Conflict of Interest The authors declare no competing interests.

References

1. den Hengst WA, Gielis JF, Lin JY, Van Schil PE, De Windt LJ, Moens AL (2010) Lung ischemia-reperfusion injury: a molecular and clinical view on a complex pathophysiological process. Am J Physiol Heart Circ Physiol 299(5):H1283-1299. https://doi.org/10.1152/ajpheart.00251.2010
2. Porteous MK, Diamond JM, Christie JD (2015) Primary graft dysfunction: lessons learned about the first 72 h after lung transplantation. Curr Opin Organ Transplant 20(5):506–514. https://doi.org/10.1097/MOT.0000000000000232
3. Pak O, Sydykov A, Kosanovic D, Schermuly RT, Dietrich A, Schroder K, Brandes RP, Gudermann T, Sommer N, Weissmann N (2017) Lung ischaemia-reperfusion injury: the role of reactive oxygen species. Adv Exp Med Biol 967:195–225. https://doi.org/10.1007/978-3-319-63245-2_12
4. Laubach VE, Sharma AK (2016) Mechanisms of lung ischemia-reperfusion injury. Curr Opin Organ Transplant 21(3):246–252. https://doi.org/10.1097/MOT.0000000000000304
5. Nakajima D, Watanabe Y, Ohsumi A, Pipkin M, Chen M, Mordant P, Kanou T, Saito T, Lam R, Coutinho R, Caldarone L, Juvet S, Martinu T, Iyer RK, Davies JE, Hwang DM, Waddell TK, Cypel M, Liu M, Keshavjee S (2019) Mesenchymal stromal cell therapy during ex vivo lung perfusion ameliorates ischemia-reperfusion injury in lung transplantation. J Heart Lung Transplant 38(11):1214–1223. https://doi.org/10.1016/j.healun.2019.07.006
6. Podesta MA, Remuzzi G, Casiraghi F (2020) Mesenchymal stromal cell therapy in solid organ transplantation. Front Immunol 11:618243. https://doi.org/10.3389/fimmu.2020.618243
7. Lazar E, Benedek T, Korodi S, Rat N, Lo J, Benedek I (2018) Stem cell-derived exosomes - an emerging tool for myocardial regeneration. World J Stem Cells 10(8):106–115. https://doi.org/10.4252/wjsc.v10.i8.106
8. Raposo G, Stoorvogel W (2013) Extracellular vesicles: exosomes, microvesicles, and friends. J Cell Biol 200(4):373–383. https://doi.org/10.1083/jcb.201211138
9. Li JW, Wei L, Han Z, Chen Z (2019) Mesenchymal stromal cells-derived exosomes alleviate ischemia/reperfusion injury in mouse

lung by transporting anti-apoptotic miR-21-5p. Eur J Pharmacol 852:68–76. https://doi.org/10.1016/j.ejphar.2019.01.022
10. Massa M, Croce S, Campanelli R, Abba C, Lenta E, Valsecchi C, Avanzini MA (2020) Clinical applications of mesenchymal stem/stromal cell derived extracellular vesicles: therapeutic potential of an acellular product. Diagnostics (Basel) 10(12):E999. https://doi.org/10.3390/diagnostics10120999
11. Quinn JJ, Chang HY (2016) Unique features of long non-coding RNA biogenesis and function. Nat Rev Genet 17(1):47–62. https://doi.org/10.1038/nrg.2015.10
12. Statello L, Guo CJ, Chen LL, Huarte M (2021) Gene regulation by long non-coding RNAs and its biological functions. Nat Rev Mol Cell Biol 22(2):96–118. https://doi.org/10.1038/s41580-020-00315-9
13. Yao RW, Wang Y, Chen LL (2019) Cellular functions of long noncoding RNAs. Nat Cell Biol 21(5):542–551. https://doi.org/10.1038/s41556-019-0311-8
14. Li J, Wei L, Han Z, Chen Z, Zhang Q (2020) Long non-coding RNA X-inactive specific transcript silencing ameliorates primary graft dysfunction following lung transplantation through microRNA-21-dependent mechanism. EBioMedicine 52:102600. https://doi.org/10.1016/j.ebiom.2019.102600
15. Jiang Y, Zhang W (2021) LncRNA ZFAS1 plays a role in regulating the inflammatory responses in sepsis-induced acute lung injury via mediating miR-193a-3p. Infect Genet Evol 92:104860. https://doi.org/10.1016/j.meegid.2021.104860
16. Pan L, Liang W, Fu M, Huang ZH, Li X, Zhang W, Zhang P, Qian H, Jiang PC, Xu WR, Zhang X (2017) Exosomes-mediated transfer of long noncoding RNA ZFAS1 promotes gastric cancer progression. J Cancer Res Clin Oncol 143(6):991–1004. https://doi.org/10.1007/s00432-017-2361-2
17. Zhang L, Yang Z, Trottier J, Barbier O, Wang L (2017) Long noncoding RNA MEG3 induces cholestatic liver injury by interaction with PTBP1 to facilitate shp mRNA decay. Hepatology 65(2):604–615. https://doi.org/10.1002/hep.28882
18. Azzalin CM, Lingner J (2006) The human RNA surveillance factor UPF1 is required for S phase progression and genome stability. Curr Biol 16(4):433–439. https://doi.org/10.1016/j.cub.2006.01.018
19. Li CH, Chang YC, Hsiao M, Liang SM (2019) FOXD1 and Gal-3 form a positive regulatory loop to regulate lung cancer aggressiveness. Cancers (Basel) 11(12):E1897. https://doi.org/10.3390/cancers11121897
20. Eslaminejad MB, Nadri S (2009) Murine mesenchymal stem cell isolated and expanded in low and high density culture system: surface antigen expression and osteogenic culture mineralization. In Vitro Cell Dev Biol Anim 45(8):451–459. https://doi.org/10.1007/s11626-009-9198-1
21. Zeng Q, Zhou Y, Liang D, He H, Liu X, Zhu R, Zhang M, Luo X, Wang Y, Huang G (2020) Exosomes secreted from bone marrow mesenchymal stem cells attenuate oxygen-glucose deprivation/reoxygenation-induced pyroptosis in PC12 cells by promoting AMPK-dependent autophagic flux. Front Cell Neurosci 14:182. https://doi.org/10.3389/fncel.2020.00182
22. Stephens RS, Rentsendorj O, Servinsky LE, Moldobaeva A, Damico R, Pearse DB (2010) cGMP increases antioxidant function and attenuates oxidant cell death in mouse lung microvascular endothelial cells by a protein kinase G-dependent mechanism. Am J Physiol Lung Cell Mol Physiol 299(3):L323-333. https://doi.org/10.1152/ajplung.00442.2009
23. Sharma AK, Charles EJ, Zhao Y, Narahari AK, Baderdinni PK, Good ME, Lorenz UM, Kron IL, Bayliss DA, Ravichandran KS, Isakson BE, Laubach VE (2018) Pannexin-1 channels on endothelial cells mediate vascular inflammation during lung ischemia-reperfusion injury. Am J Physiol Lung Cell Mol Physiol 315(2):L301–L312. https://doi.org/10.1152/ajplung.00004.2018
24. Xu Y, Li X, Cheng Y, Yang M, Wang R (2020) Inhibition of ACSL4 attenuates ferroptotic damage after pulmonary ischemia-reperfusion. FASEB J 34(12):16262–16275. https://doi.org/10.1096/fj.202001758R
25. Wang M, Ji P, Wang R, Zhao L, Xia Z (2012) TRPV1 agonist capsaicin attenuates lung ischemia-reperfusion injury in rabbits. J Surg Res 173(1):153–160. https://doi.org/10.1016/j.jss.2010.08.053
26. Luo N, Liu J, Chen Y, Li H, Hu Z, Abbott GW (2018) Remote ischemic preconditioning STAT3-dependently ameliorates pulmonary ischemia/reperfusion injury. PLoS One 13(5):e0196186. https://doi.org/10.1371/journal.pone.0196186
27. Silva AM, Teixeira JH, Almeida MI, Goncalves RM, Barbosa MA, Santos SG (2017) Extracellular Vesicles: Immunomodulatory messengers in the context of tissue repair/regeneration. Eur J Pharm Sci 98:86–95. https://doi.org/10.1016/j.ejps.2016.09.017
28. Dong H, Wang W, Chen R, Zhang Y, Zou K, Ye M, He X, Zhang F, Han J (2018) Exosome-mediated transfer of lncRNASNHG14 promotes trastuzumab chemoresistance in breast cancer. Int J Oncol 53(3):1013–1026. https://doi.org/10.3892/ijo.2018.4467
29. Chen Q, Liu Y, Ding X, Li Q, Qiu F, Wang M, Shen Z, Zheng H, Fu G (2020) Bone marrow mesenchymal stem cell-secreted exosomes carrying microRNA-125b protect against myocardial ischemia reperfusion injury via targeting SIRT7. Mol Cell Biochem 465(1–2):103–114. https://doi.org/10.1007/s11010-019-03671-z
30. Zhang Y (2020) lncRNA ZFAS1 improves neuronal injury and inhibits inflammation, oxidative stress, and apoptosis by sponging miR-582 and upregulating NOS3 expression in cerebral ischemia/reperfusion injury. Inflammation 43(4):1337–1350. https://doi.org/10.1007/s10753-020-01212-1
31. Janakiraman H, House RP, Gangaraju VK, Diehl JA, Howe PH, Palanisamy V (2018) The Long (lncRNA) and short (miRNA) of It: TGFbeta-mediated control of RNA-binding proteins and noncoding RNAs. Mol Cancer Res 16(4):567–579. https://doi.org/10.1158/1541-7786.MCR-17-0547
32. Dehecq M, Decourty L, Namane A, Proux C, Kanaan J, Le Hir H, Jacquier A, Saveanu C (2018) Nonsense-mediated mRNA decay involves two distinct Upf1-bound complexes. EMBO J 37 (21). e99278 https://doi.org/10.15252/embj.201899278
33. Han S, Cao D, Sha J, Zhu X, Chen D (2020) LncRNA ZFPM2-AS1 promotes lung adenocarcinoma progression by interacting with UPF1 to destabilize ZFPM2. Mol Oncol 14(5):1074–1088. https://doi.org/10.1002/1878-0261.12631
34. Hannenhalli S, Kaestner KH (2009) The evolution of Fox genes and their role in development and disease. Nat Rev Genet 10(4):233–240. https://doi.org/10.1038/nrg2523
35. Mu L, Zhang J, Wu Z, Huang J, Cui Y (2022) FOXD1 Regulates the sensitivity of cetuximab by regulating the expression of EGFR in head and neck squamous cell cancer. J Healthc Eng 2022:6108241. https://doi.org/10.1155/2022/6108241
36. Bond KH, Fetting JL, Lary CW, Emery IF, Oxburgh L (2021) FOXD1 regulates cell division in clear cell renal cell carcinoma. BMC Cancer 21(1):312. https://doi.org/10.1186/s12885-021-07957-8
37. Lin L, Peng SL (2006) Coordination of NF-kappaB and NFAT antagonism by the forkhead transcription factor Foxd1. J Immunol 176(8):4793–4803. https://doi.org/10.4049/jimmunol.176.8.4793

38. Meng F, Liu Y, Chen Q, Ma Q, Gu S, Cui R, Cao R, Zhao M (2020) METTL3 contributes to renal ischemia-reperfusion injury by regulating Foxd1 methylation. Am J Physiol Renal Physiol 319(5):F839–F847. https://doi.org/10.1152/ajprenal.00222.2020
39. Perillo NL, Marcus ME, Baum LG (1998) Galectins: versatile modulators of cell adhesion, cell proliferation, and cell death. J Mol Med (Berl) 76(6):402–412. https://doi.org/10.1007/s001090050232
40. Liu FT (2005) Regulatory roles of galectins in the immune response. Int Arch Allergy Immunol 136(4):385–400. https://doi.org/10.1159/000084545
41. Liu FT, Hsu DK (2007) The role of galectin-3 in promotion of the inflammatory response. Drug News Perspect 20(7):455–460. https://doi.org/10.1358/dnp.2007.20.7.1149628
42. Sunil VR, Francis M, Vayas KN, Cervelli JA, Choi H, Laskin JD, Laskin DL (2015) Regulation of ozone-induced lung inflammation and injury by the beta-galactoside-binding lectin galectin-3. Toxicol Appl Pharmacol 284(2):236–245. https://doi.org/10.1016/j.taap.2015.02.002
43. Levin BS, Chang MG, Bittner EA (2021) Teleguidance technology for endotracheal intubation: a scoping review. Crit Care Explor 3(12):e0582. https://doi.org/10.1097/CCE.0000000000000582